Received: 9 March 2020 | Revised: 23 April 2020 | Accepted: 24 April 2020

DOI: 10.1002/pol.20200153

ORIGINAL ARTICLE

JOURNAL OF POLYMER SCIENCE WILEY

Asymmetric chain-growth synthesis of polyisocyanide with chiral nickel precatalysts

Sandra Schraff[1] | **Nora M. Kreienborg**[2] | **Jens Trampert**[1] | **Yu Sun**[3] | **Andreas Orthaber**[4] | **Christian Merten**[2] | **Frank Pammer**[1]

[1]Institute of Organic Chemistry II and Advanced Materials, University of Ulm, Ulm, Germany

[2]Organic Chemistry II, Ruhr University Bochum, Faculty of Chemistry and Biochemistry, Bochum, Germany

[3]Fachbereich Chemie, Anorganische Chemie, Technische Universität Kaiserslautern, Kaiserslautern, Germany

[4]Department of Chemistry—Ångström laboratories, Uppsala University, Uppsala, Sweden

Correspondence
Frank Pammer, Institute of Organic Chemistry II and Advanced Materials, University of Ulm, Albert-Einstein-Allee 11, 89081 Ulm, Germany.
Email: frank.pammer@uni-ulm.de

Christian Merten, Organic Chemistry II, Ruhr University Bochum, Faculty of Chemistry and Biochemistry, Universitätsstrasse 150, 44801 Bochum, Germany.
Email: christian.merten@ruhr-uni-bochum.de

Funding information
Deutsche Forschungsgemeinschaft, Grant/Award Numbers: FP 2217/3-1, EXC-2033,ME4267/5-1; Verband der Chemischen Industrie, Grant/Award Numbers: Liebig Scholarship, Doctoral Scholarship

Abstract

Nickel(II)-aryl complexes [(L_2)Ni(Ar)Br] bearing either chiral phosphine ligands (L_2 = *RR*- or *SS*-DIPAMP, Ar = *ortho*-anisyl), or a chiral aryl-group have been prepared, and their structural optical an chiroptical properties have been characterized. Enantiomeric pairs of both catalysts have been used for the asymmetric polymerization of different isocyanides (**M1**, **M2**, **M3**), to give well defined polyisocyanides (**P1**, **P2**, **P3**). Their polymerization behavior has been studied, which confirmed chain-growth polymerization in all cases. The asymmetric induction has been verified by circular dichroism spectroscopy on enantiomeric pairs of all three polymers.

KEYWORDS

atropisomers, CD-spectroscopy, DIPAMP, helical polymers, chain-growth polymerization, fulvenes, nickel catalysts, polyisocyanides, isocyanides

1 | INTRODUCTION

The chemistry of alkyl- and aryl-isocyanides is well-developed, since these building blocks are commonly employed

Sandra Schraff and Nora M. Kreienborg contributed equally to this work.

in organic syntheses,[1,2] and as ligands in organometallic coordination chemistry.[3] Likewise, their polyaddition products, polyisocyanides (**PIC**s), are being investigated since the 1970s[4] and have attracted growing interest with the recent development of new polymerization catalysts that allow their controlled synthesis by quasi-living polymerization.[5] This has opened an access to the preparation of a variety of block copolymers including **PIC**s as co-blocks to conjugated polymers.[6] Still, reports of **PIC**s as electronic materials are comparatively rare. **PIC**s equipped with redox-active functional groups that showed reversible electrochromic behavior, were reported.[7,8] In our group, we have recently developed **PIC**s bearing redox-active fulvenyl-groups, on which we report herein.[9,10,26]

An intriguing property of **PIC**s is the fact that their sterically congested main-chain cannot adopt of coplanar conformation. Instead, the polyimine backbone adopts a helical structure in which approximately four repeat-units complete one full turn (4_1-helix).[4,11] **PIC**s are thus intrinsically chiral polymers. Hence, significant efforts have been made to isolate and prepare enantiomerically pure or enriched **PIC**s. For instance, poly(*tert*-butylisocyanide) (P[^{t}BuNC]) forms very stable helices, the enantiomers of which can be separated chromatographically.[12] Other **PIC**s without chiral side-chains can self-organize enantioselectively in a chiral environment.[13] Still, the most common approach is polymerization of homochiral monomers bearing defined asymmetric centers, either neat[14] or as co-monomers in random copolymers.[7,8,15] Notably, the presence of defined stereogenic centers does not necessarily result in a predefined screw-sense selectivity. Instead, the absolute configuration of the polymer can be influenced by the solvent and preparation conditions.[16]

Another synthetic strategy is the direct asymmetric synthesis of **PIC**s through polymerization of achiral monomers. This can be achieved for instance with chiral palladium catalysts[17] or with nickel catalysts that feature either chiral counter ion (**A**, Chart 1),[18,19] or via the use of chiral initiators (**B**).[20,21] For instance, when the asymmetric polymerization is induced by *R*-1-phenylethylamine as initiator P(^{t}BuNC) is formed in up to 62% enantiomeric excess (**B**).[22] More recently, it has been shown that the aryl-group in aryl-nickel(II) complexes can also act as initiators for polyisocyanides synthesis. This finding has been exploited in the preparation of block-copolymers,[23–27] and in the asymmetric synthesis of polyisocyanides through introduction of chiral aryl-groups into nickel(II) precatalysts (**C**).[28]

We recently reported the preparation of three fulvenyl-functionalized isocyanides (**M1**–**M3**, Scheme 1), and their polymerization to the corresponding **PIC**s (**P1**–**P3**).[9,10,26] In the present paper, we report two new enantiomeric pairs of precatalysts (**C1-*RR*/C1-*SS***, and **C2-*R*/C2-*S***) that facilitate chain-growth polymerization **M2**, and we successfully employed them in the asymmetric polymerization of **M1** through **M3**. Additionally, these results provide evidence that the polymers indeed adopt a helical structure, and they indicate that both the structure of the polymer backbone and the fulvenyl-groups remain intact in the polymers.

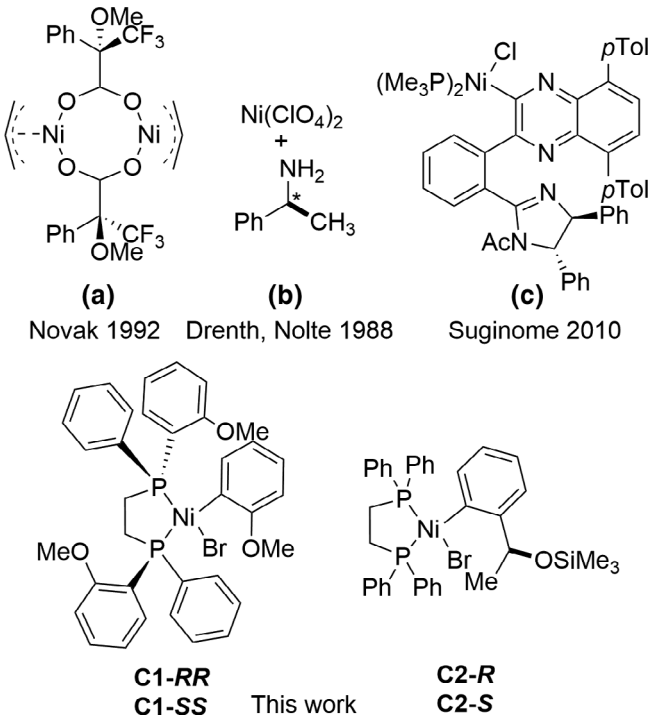

CHART 1 Catalyst systems for the asymmetric polymerization of isocyanides

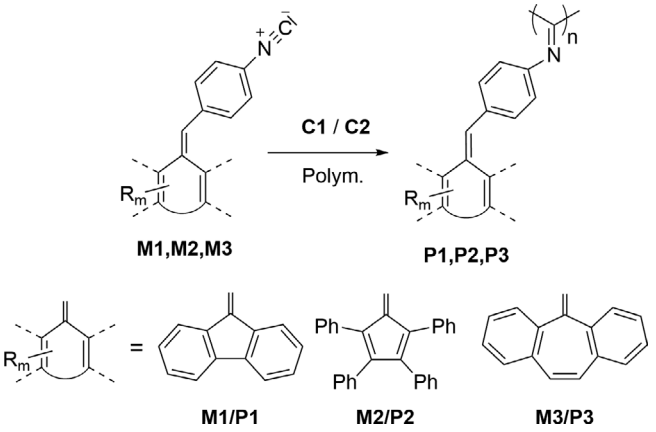

SCHEME 1 Monomers and polymers discussed in this article

2 | EXPERIMENTAL

2.1 | Materials and instrumentation

All reactions and manipulations of sensitive compounds were carried out under an atmosphere of prepurified argon

using either Schlenk techniques or an inert-atmosphere glovebox (Sylatech GB 1500-E), except for UV–vis- and CD-spectroscopy measurements. Toluene, Et_2O, THF and dichloromethane were purified using a solvent purification system (MBraun; alumina/copper columns for hydrocarbon solvents). Hexane and benzene were dried by distillation from CaH_2 under argon atmosphere prior to use. Monomers **M1**, **M2**, and **M3**, were prepared according to published procedures.[9] Other reagents were commercially available (Aldrich, Acros, Alfa Aesar) and were either used as obtained or purified by standard procedures.[29] ^{1}H-, ^{13}C-, and ^{31}P-NMR spectra were recorded at 293 K on a Bruker Avance DRX 400 (400 MHz) spectrometer or a Bruker Avance 500 AMX (500 MHz). Solution ^{1}H and ^{13}C NMR spectra were referenced internally to the residual signals solvent.[30] ^{31}P NMR spectra were referenced externally to 85% H_3PO_4 $_{(aq)}$. Individual signals are referred to as singlet (s), doublet (d), triplet (t), multiplet (m), centro-symmetrical multiplet (m_c), and broadened (br). High-resolution mass spectrometry measurements were performed on a Bruker SolariX FTMS using MALDI (Matrix Assisted Laser Desorption Ionization). *Trans*-2-[3-(4-*tert*-butylphenyl)-2-methyl-2-propenylidene]malononitrile (DCTB) or 2,5-dihydroxybenzoic acid (DHB) was used as matrix in MALDI measurements. UV–visible absorption spectra were acquired on a Perkin Elmer Lambda 19 UV–vis/NIR spectrometer and a Perkin Elmer LS 55 fluorescence spectrometer, respectively. Deconvolution of UV–vis spectra were performed with OriginPro 2017G. Gel permeation chromatography UV analyses (GPC-UV) with THF as eluent were performed on a Merck Hitachi LaChrom GPC system, equipped with an L-7100 HPLC pump, L-7420 UV–vis detector and three columns (PSS SDV 10^3 Å, 10^4 Å, and 10^5 Å). The columns were kept in a column heater at 35 °C and were calibrated with polystyrene standards (Polymer Laboratories).

Elemental analyses were performed on an Elemental Vario EL analyzer. Melting points were measured on a Büchi M-565 melting point apparatus with a heating rate of 1 °C/min or on a Mettler Toledo differential scanning calorimeter, model DSC 823e.

2.1.1 | CD-spectroscopy

The UV–VIS and CD spectra were recorded on an Applied Physics Chirascan™-plus CD Spectrometer at room temperature in a quartz cuvette with 1 cm path length.

2.1.2 | Crystallography

X-ray diffraction intensities were collected either on an Agilent Technologies SuperNova single-crystal X-ray diffractometer. Data collection was performed at 150 K using either Cu- or Mo-Kα radiation, and the structures were solved using direct methods (SIR92[31] or Shlexs-2014[32]), completed by subsequent difference Fourier syntheses, and refined by full-matrix least-squares procedures. CCDC 1981165 and CCDC 1981168 contain the supplementary crystallographic data for **C3** and **C2-*S***, respectively. These data can be obtained free of charge from the Cambridge Crystallographic Data Centre via www.ccdc.cam.ac.uk/data_request/cif.

2.1.3 | Computational details

Quantum chemical calculations were performed on the bwForCluster JUSTUS at the University of Ulm, using release C.01 of the Gaussian16 program package.[33] Geometry optimizations were performed at the B3LYP-D3/TZVP-level. Pseudopotentials mdf10 and mwb28 were used for Ni and Br, respectively. The converged structures were found to be local energetic minima, as established by frequency calculations. The rotational barrier was estimated via relaxed 360° scan of the dihedral angle Br–Ni–C–C^{OMe} starting from the optimized geometry in either the forward (+) or backward (−) direction. The structures of an oligomeric model of **P1 P2** (**$P2_{8M}$**, 8mer, *M*-helix) has been optimized at the B3LYP-D3/6-31G(d,p) level. Only an *isotactic* structure with equal configuration on all imine-nitrogens and fulvene-bonds has been optimized. Its optical properties have been simulated by time-dependent DFT calculations using CAM-B3LYP/6-31G(d,p).

2.1.4 | Synthesis of R- and S-O-trimethylsilyl-1-(2-bromophenyl)-ethanol (S1-R/S1-S)

A Schlenk tube under Argon atmosphere was charged with 355 mg of *R*-(+)-1-(2-bromophenyl)-ethanol (1.76 mmol, 1.0 eq.), 4.40 ml of dry toluene, and 550 µl (3.53 mmol, 2.0 eq.) of 1,8-Diazabicyclo[5.4.0]undec-7-ene (DBU), and 300 µl (2.29 mmol, 1.3 eq.) of trimethylsilyl chloride were added last. The mixture was stirred for 2 hr at ambient temperature, and all volatiles were subsequently removed. The residue was taken up in diethyl ether and the organic phases were washed with water several times, until the pH was neutral. The organic phase was separated and dried over Na_2SO_4. Evaporation of the solvent yielded **S1-*R*** in 88% yield (423 mg, 1.55 mol) as a colorless oil. **S1-*S*** was synthesized analogously in 78% yield. Analytical data for **S1-*R***: ^{1}H-NMR (400 MHz, $CDCl_3$): δ = 7.60 (dd, J_{HH} = 7.8, 1.8 Hz, 1H), 7.47 (dd,

J_{HH} = 8.0, 1.2 Hz, 1H), 7.33–7.29 (m, 1H), 7.11–7.07 (m, 1H), 5.19–5.14 (q, J_{HH} = 6.3 Hz, 1H), 1.40 (d, $^{3}J_{HH}$ = 6.3 Hz, 3H), 0.08 (s, 9H, —Si[CH_3]$_3$) ppm. ^{13}C-NMR (101 MHz, $CDCl_3$): δ = 145.8, 132.4, 128.4, 127.8, 127.6, 121.0, 69.7, 25.6, 0.12 ppm. Elemental analysis for $C_{11}H_{17}BrOSi$ (%): calcd. C 48.35, H 6.27; exp. C 47.95, H 6.08.

2.1.5 | Synthesis of aryl-nickel complexes—General procedure

Example for the synthesis of [*SS*-dipamp)Ni(II)(*ortho*-anisyl) bromide] (**C1-*SS***): Under argon atmosphere Ni(cod)$_2$ (30.0 mg, 109 μmol, 1.0 eq.) and PPh_3 (63.0 mg, 240 μmol, 2.2 eq.) were dissolved in 1.5 ml of dry toluene. The resulting dark red solution was stirred at ambient temperature for 15 min. Subsequently, 2-bromoanisole (70 μl, 105 mg, 545 μmol, 5.0 eq.) was added, and the mixture was stirred for 2 hr, to give a brownish-yellow solution of [(PPh_3)$_2$Ni(*ortho*-anisyl)Br] (**C3**). To this mixture, 50.0 mg (109 μmol, 1.0 eq.) of (*R*,*R*)-DIPAMP were then added, and the reaction mixture was stirred for an additional 17 hr. To the resulting suspension, 1.0 ml of dry *n*-hexane was added and the precipitate was isolated by centrifugation. The yellow solid was washed once with a toluene/*n*-hexane mixture (1:2, vol/vol), and once with neat *n*-hexane. Drying under vacuum yielded **C1-*SS*** as yellow powder in a yield of 94% (72.0 mg, 102 μmol). Single crystals of **C3** were obtained by layering the intermediate solution with hexane. **C1-*SS***: ^{31}P-NMR (400 MHz, C_6D_6): δ = 57.9 (d, J_{PP} = 25.4 Hz), 51.1 (d, J_{PP} = 25.7 Hz), 43.7 (d, J_{PP} = 25.7 Hz), 38.9 (d, J_{PP} = 25.7 Hz) ppm. ^{31}P-NMR (162 MHz, THF-d_8): δ = 59.7 (d, J_{PP} = 26.4 Hz), 53.55 (d, J_{PP} = 26.4 Hz), 45.4 (d, J_{PP} = 26.7 Hz), 40.9 (d, J_{PP} = 26.7 Hz) ppm. ^{1}H NMR (400 MHz, C_6D_6): δ = 9.66 (ddd, J_{HH} = 1.4 Hz/7.5 Hz/15.0 Hz, 1H), 8.55 (t, $^{3}J_{HH}$ = 8.2 Hz, 1 H), 8.42 (m_c, 1 H), 8.02 (m_c, 1 H), 8.81 (m_c, 2 H), 7.67 (m_c, 0.6 H, minor isomer), 7.48 (t, $^{3}J_{HH}$ = 6.5 Hz, 1 H), 7.20–7.32 (m, 3.5 H)*, 7.14–7.08* (m, 2.8 H), 6.90–7.06 (m, 4.6 H), 6.76–6.90 (m, 5.2 H), 6.67 (t, $^{3}J_{HH}$ = 7.4 Hz, 0.6 H, minor isomer), 6.52–6.60 (m, 2 H), 6.45 (dd, J_{HH} = 2.3 Hz/8.1 Hz, 1H), 6.36 (dd, J_{HH} = 4.2 Hz/8.2 Hz, 1H), 6.27 (t, $^{3}J_{HH}$ = 7.4 Hz, 0.6 H, minor isomer), 6.21 (dd, J_{HH} = 5.2 Hz/8.0 Hz, 0.4 H, minor isomer), 6.11 (dd, J_{HH} = 2.1 Hz/7.7 Hz, 1H), 6.01 (m_c, 0.4 H, minor isomer), 3.49 (s, 1.5 H, OMe, minor isomer), 3.29 (s, 3 H, OMe), 3.25 (s, 1.5 H, OMe, minor isomer), 3.11 (s, 3 H, OMe), 3.04 (s, 3 H, OMe), 2.79 (s, 1.5 H, OMe, minor isomer), 2.62–2.74 (m, 0.6 H, DIPAMP-CH_2), 2.49–2.58 (m, 0.5 H, DIPAMP-CH_2), 2.39–2.48 (m, 0.5 H, DIPAMP-CH_2), 2.26–2.36 (m, 0.6 H, DIPAMP-CH_2), 2.16–2.24 (m, 0.5 H, DIPAMP-CH_2), 1.89–2.06 (m, 2 H, DIPAMP-CH_2), 1.79–1.89 (m, 0.5 H, DIPAMP-CH_2), 1.59–1.76 (m, 1 H, DIPAMP-CH_2) ppm. ^{1}H NMR (400 MHz, THF-d_8): δ = 9.12 (ddd, J_{HH} = 1.2 Hz/7.4 Hz/13.6 Hz, 1H), 8.58 (t, $^{3}J_{HH}$ = 7.3 Hz, 1 H), 8.49 (t, $^{3}J_{HH}$ = 8.4 Hz, 1 H), 8.02 (m_c, 1 H), 8.12 (dd, J_{HH} = 7.5 Hz/12.0 Hz, 1H), 7.74–7.85 (m, 0.5 H), 7.65–7.72 (m, 2.5 H), 7.55–7.64 (m, 3.5 H), 7.48 (q, $^{3}J_{HH}$ = 7.5 Hz, 2 H), 3.37–7.44 (m, 0.5 H), 7.30–7.37 (m, 4 H), 7.20 (m_c, 1 H), 6.92–7.14 (m, 12 H), 6.78–6.85 (m, 1 H), 6.70–6.78 (m, 1 H), 6.43 (t, $^{3}J_{HH}$ = 7.3 Hz, 1 H), 6.33 (t, $^{3}J_{HH}$ = 7.5 Hz, 0.5 H), 6.21–6.30 (m, 3 H), 5.84 (dd, J_{HH} = 2.3 Hz/7.7 Hz, 1H), 5.72 (dd, J_{HH} = 2.3 Hz/7.8 Hz, 0.5 H), 3.92 (s, 1.5 H, OMe, minor isomer), 3.60* (s, 3 H, OMe, major isomer), 3.53 (s, 3 H, OMe, major isomer), 3.35 (s, 1.5 H, OMe, minor isomer), 3.29 (s, 3 H, OMe, major isomer), 3.21 (s, 1.5 H, OMe, minor isomer), 2.75–2.87 (m, 0.5 H, DIPAMP-CH_2)), 2.60–2.68 (m, 0.5 H, DIPAMP-CH_2), 2.49–2.60 (m, 1.5 H, DIPAMP-CH_2), 2.40–2.47 (m, 0.5 H, DIPAMP-CH_2), 2.15–2.25 (m, 1 H, DIPAMP-CH_2), 1.95–2.04 (m, 1 H, DIPAMP-CH_2), 1.75–1.86 (m, 1 H, DIPAMP-CH_2). *Superimposed with solvent signal. HR-FTMS (MALDI, matrix DCTB, positive Mode) for $C_{35}H_{35}NiO_3P_2$ [M−Br]$^+$: calcd. m/z = 623.1415 u; exp: m/z = 623.1411 u ([M−Br]$^+$).

2.1.6 | C1-RR

Synthesis carried out analogous to that of **C1-*SS***. Yield: 90% (46.0 mg, 65.3 μmol) based on 20.0 mg (72.7 μmol) of Ni(cod)$_2$.

2.1.7 | C2-S ([(dppe)nickel(II)(ortho-[S-1-trimethylsilyloxyethyl]-phenyl) bromide]

Synthesis and workup were carried out analogous to **C1-*SS***, except that after addition of 5.0 eq. of 1-bromo-2-(*S*-1-trimethylsilyloxyethyl)-benzene the reaction mixture was stirred for 20 hr prior to addition of DPPE. Yield: 81% (90.0 mg, 123 μmol) based on 42.0 mg (153 μmol) of Ni(cod)$_2$. Single crystals of **C2-*S*** were obtained by diffusion of pentane into a solution of the catalyst in toluene. ^{31}P-NMR (162 MHz, C_6D_6): δ = 51.8 (d, J_{PP} = 17.5 Hz), 50.7 (d, J_{PP} = 18.1 Hz), 36.5 (d, J_{PP} = 17.4 Hz), 36.1 (d, J_{PP} = 18.4 Hz) ppm. ^{1}H NMR (400 MHz, THF-d_8): δ = 8.22–8.34 (m, 5.5 H), 8.18 (m_c, 1.5 H), 8.03 (m_c, 1 H), 7.71–7.80 (m, 2 H), 7.64–7.72 (m, 2.5 H), 7.43–7.60 (m, 13 H), 7.30–7-43 (m, 6.5 H), 7.18–7.28 (m, 2.5 H), 6.94–7.04 (m, 4 H), 6.81 (d, $^{3}J_{HH}$ = 7.0 Hz, 1 H), 6.72 (t, $^{3}J_{HH}$ = 8.8 Hz, 1.5 H), 6.52–6.66 (m, 4.5 H), 6.47 (t, $^{3}J_{HH}$ = 7.0 Hz,0.5 H), 5.91 (q, $^{3}J_{HH}$ = 6.2 Hz, 0.5 H), 5.44 (q, $^{3}J_{HH}$ = 6.0 Hz, 1 H), 2.69–2.79 (m, 0.5 H), 2.56–2.66 (m, 1 H), 2.26–2.54 (m, 5 H), 2.12–2.26 (m, 1 H),

1.52–1.66 (m, 1 H), 1.56 (d, $^3J_{HH}$ = 6.1 Hz, 3 H, CHCH_3), 1.34–1.48 (m, 1 H), 0.76 (d, $^3J_{HH}$ = 6.2 Hz, 2.2 H, CHCH_3), 0.02 (s, 6.8 H, $SiMe_3$), −0.18 (s, 9 H, $SiMe_3$). HR-FTMS (MALDI, matrix DCTB, positive Mode) for $C_{37}H_{41}BrNiOP_2Si$: calcd. m/z = 729.0939 u $[M]^+$, 649.1755 u $[M-Br]^+$; exp: m/z = 649.1747 u ($[M-Br]^+$).

2.1.8 | C2-R ([(dppe)nickel(II)(ortho-[R-1-trimethylsilyloxyethyl]-phenyl) bromide])

Synthesis and workup were carried out analogous to **C1-*SS***, except that after the addition of 5.0 eq. of 1-bromo-2-(*R*-1-trimethylsilyloxyethyl)-benzene the reaction mixture was stirred for 20 hr prior to addition of DPPE. Yield: 72% (80.0 mg, 110 μmol) based on 42.0 mg (153 μmol) of $Ni(cod)_2$.

2.1.9 | Polymerization experiments—General procedure

Solutions of the respective monomers with concentrations of ca. 0.3 mM were prepared in the solvent mixtures specified in Table 1 of the main manuscript. Then, 1 mol % of the Ni-catalysts dissolved in THF were injected into the stirred monomer-solutions. The reaction mixtures were stirred at ambient temperature for 16 hr followed by removal of the solvent under vacuum. The residue was washed by dispersion in methanol and was recovered by centrifugation. The same process was repeated in *n*-hexane, and the recovered solids were dried in vacuum. For CD-spectroscopy, samples were dissolved in THF immediately prior to measurement.

2.1.10 | Polymerization kinetics experiments

In a glove box under argon atmosphere, monomer **M2** (20 mg, 41.4 μmol) and 2 mg of the internal standard Ph_2O were dissolved in 1 ml of dry toluene, and a reference sample (t = 0 min) of the mixture was taken. Catalysts **C1-*SS*** and **C2-*S*** (0.25 mol% dissolved in a 10/1 mixture of toluene and THF) were then quickly injected into the stirred solution. At intervals, samples (ca. 20 μl) were taken with a single use pipette, and the sample solutions where quenched by immediate absorption onto sand. The samples were taken out of the glovebox, and ca. 20 μl ml of Methanol was added to fully quench the polymerization. The sand was extracted with 1 ml of dichloromethane, the extracts were filtered, and the filtrates were analyzed by GPC-UV. Conversion of **M2** was determined from the **M2**/Ph_2O-ratio derived from integration of the GPC-UV chromatograms.

TABLE 1 Asymmetric polymerization results with **C1-*RR*/C1-*SS*** and **C2-*R*/C2-*S***

Nr.	Monomer	Solvent[a]	Catalyst[b]	Polymer	M_n (kg/mol)[b]	DP_n	PDI	$\lambda_{\Delta\varepsilon}$max (nm)	CD ($10^{-3\circ}$ M^{-1} cm^{-1}]
1	**M1**	Et_2O/toluene	**C1-*RR***	$\mathbf{P1}^{\mathbf{C1\text{-}RR}}$	5.3	19	1.09	388	+86.9
2	**M1**	MeCN/toluene	**C1-*RR***	$\mathbf{P1}^{\mathbf{C1\text{-}SS}}$	5.2	19	1.12		+59.4
3	**M1**	Et_2O/toluene	**C1-*SS***	$\mathbf{P1}^{\mathbf{C1\text{-}RR}}$	4.0	14	1.14		−85.5
4	**M1**	MeCN/toluene	**C1-*SS***	$\mathbf{P1}^{\mathbf{C1\text{-}SS}}$	4.8	17	1.09		−62.6
5	**M2**	Et_2O/toluene	**C1-*RR***	$\mathbf{P2}^{\mathbf{C1\text{-}RR}}$	6.8	14	1.07	451	+6.6
6	**M2**	MeCN/toluene	**C1-*RR***	$\mathbf{P2}^{\mathbf{C1\text{-}RR}}$	6.9	14	1.07		+5.7
7	**M2**	Et_2O/toluene	**C1-*SS***	$\mathbf{P2}^{\mathbf{C1\text{-}SS}}$	4.1	8	1.04		−12.5
8	**M2**	MeCN/toluene	**C1-*SS***	$\mathbf{P2}^{\mathbf{C1\text{-}SS}}$	4.5	9	1.06		−20.0
9	**M3**	Et_2O/toluene	**C1-*RR***	$\mathbf{P3}^{\mathbf{C1\text{-}RR}}$	3.4	11	1.04	392	+80.1
10	**M3**	MeCN/toluene	**C1-*RR***	$\mathbf{P3}^{\mathbf{C1\text{-}RR}}$	3.5	11	1.06		—
11	**M3**	Et_2O/toluene	**C1-*SS***	$\mathbf{P3}^{\mathbf{C1\text{-}RR}}$	3.1	10	1.05		−174.5
12	**M3**	MeCN/toluene	**C1-*SS***	$\mathbf{P3}^{\mathbf{C1\text{-}RR}}$	3.0	10	1.06		—
13	**M2**	Et_2O/toluene	**C2-*R***	$\mathbf{P2}^{\mathbf{C2\text{-}R}}$	13.2	27	1.17	400	−9.4
14	**M2**	Et_2O/toluene	**C2-*S***	$\mathbf{P2}^{\mathbf{C2\text{-}S}}$	11.1	23	1.14		+11.1

[a]Solvent ratio Et_2O or MeCN versus toluene 2:1 vol/vol.
[b]Catalyst loading: 1 mol%.
[c]Determined by GPC in THF at 35 °C relative to polystyrene standards.

3 | RESULTS AND DISCUSSION

3.1 | Precatalysts synthesis and characterization

In our initial efforts to prepare optically active batches of the above polymers, **M2** was polymerized with using $Ni(OTf)_2$ and *R*-1-phenylethylamine analogous to the procedure reported by Nolte and Drenth.[22] However, these experiments only furnished optically inactive polymers. We therefore changed our strategy and prepared the chiral precatalysts **C1-*RR*/C1-*SS*** bearing chiral *RR*- and *SS*-DIPAMP-ligands (*R*,*R*-/*S*,*S*-1,2-(bis[*ortho*-anisylphenylphosphino]ethane) and the complexes **C2-*R*/C2-*S***, bearing chiral aryl-groups on the metal center (Chart 1). The complexes were prepared via a modified known procedure (Scheme 2).[34] Through partial ligand exchange with PPh_3, followed by oxidative addition of aryl-halides, $Ni^0(cod)_2$ was converted into to an intermediate complex of the type $[(PPh_3)_2Ni(Ar)Br]$, bearing either an *ortho*-anisyl-group (**C3**), or a homochiral *ortho*-(1-trimethylsilyloxyethyl)-phenyl-group (**C3***) on the metal center. The PPh_3-ligands were then substituted either by DIPAMP to give **C1-*RR*** and **C1-*SS***, or by DPPE (1,2-bisdiphenylphosphinoethane) to give **C2-*R*** and **C2-*S***. This one-pot procedure yielded the four complexes in good to excellent yields. All compounds were characterized by ^1H, ^{13}C, and ^{31}P NMR, and high-resolution mass spectroscopy. Single crystals suitable for X-ray diffraction were also obtained of **C2-*S*** (Figure 1a) and of the intermediate complex **C3** (Figure 1b).

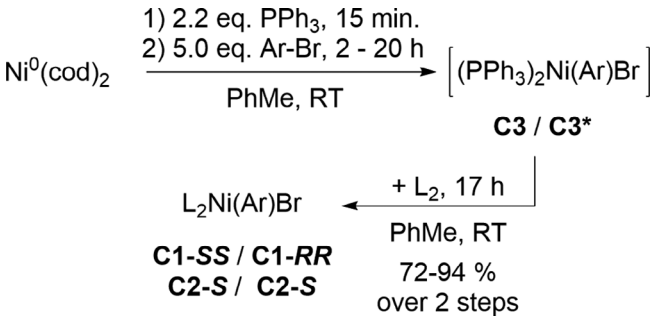

SCHEME 2 Catalyst synthesis. **C3**/**C1**: Ar = *ortho*-anisyl, **C3***/**C2**: Ar = *R*-/*S*-1-trimethylsilyloxyethyl)-phenyl, **C1**: L_2 = *RR*-/*SS*-DIPAMP, **C2**: L_2 = DPPE. cod: 1,5-cyclooctadiene

C2-*S* crystallized in the chiral monoclinic space group $P2_1$ with two crystallographically independent molecules in the unit cell (Figure 1a). The structure confirms the absolute configuration at the asymmetric carbon atom of **C2-*S***. In the crystal structures of both **C2-*S*** and **C3** (Figure 1b), the ligands adopt a near ideal square planar coordination geometry around the metal center. However, for **C3** the phosphine ligands adopt a *trans* configuration, while the chelating DPPE ligand in **C2-*S*** enforces a *cis* configuration of the complex. In both complexes, the aryl-moiety connected to nickel stands nearly perpendicular to the coordination plane (**C2-*S***: (Br–Ni–C–CR) = 84.2 (1)°/89.9 (1)°, **C3**: (P–Ni–C–CO) = 90.0(0)°). The ideal 90° orientation of the anisyl-ring in **C3** is owed to the symmetry of the unit cell, but likely also originates

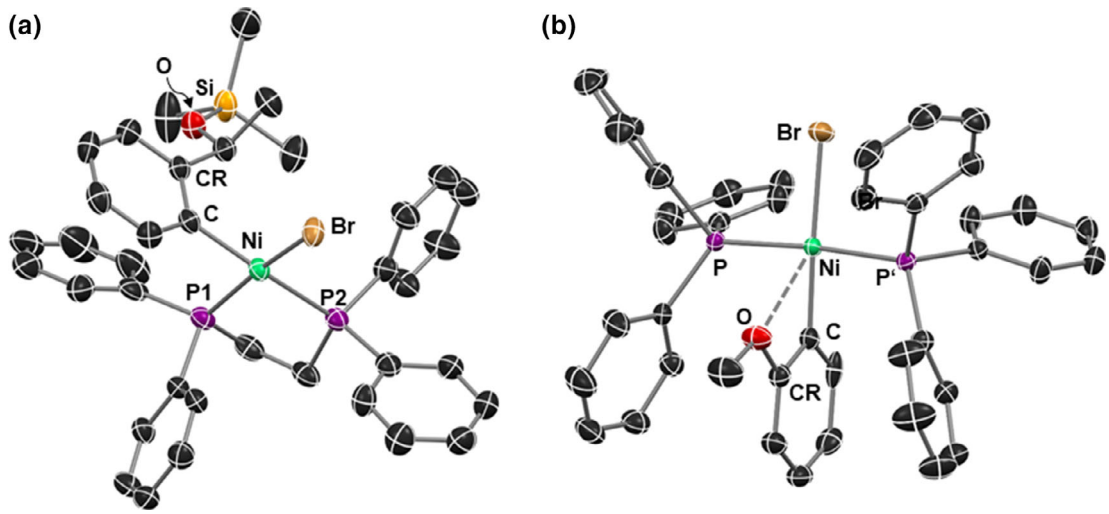

FIGURE 1 Crystal structures of (a) **C2-*S*** and (b) **C3**. Ellipsoids shown at 55% probability level. Only one of two crystallographically independent molecules in the unit cell of **C2-*S*** is shown. Hydrogen atoms have been omitted for clarity. Selected bond lengths (Å) and angles (°) for **C2-*S*** (molecule 1/molecule 2): P1-Ni 2.119(1)/2,124(1), P2-Ni 2.222(1)/2.222(1), Br–Ni 2.334(1)/2.327(1), C–Ni 1.924(4)/1.924 (4), Br–Ni-C1-C2 100.8(3)/102.2(3), P1-Ni-P2 86.3(1)/87.4(1), P–Ni–Br 96.1(1)/95.0(1), Br–Ni–C 93.6(1)/92.5(1), C–Ni–P 86.7(1)/87.1(1). Selected bond lengths (Å) and angles (°) for **C3**: P–Ni 2.197(1), Br–Ni 2.342(1) C–Ni 1.884(3) P–Ni–C–CO: 87.8(2), Br–Ni–C 175.3(1) P–Ni–P′ 174.0(1), P–Ni–C 87.9(1) P–Ni–Br 92.2(1) [Color figure can be viewed at wileyonlinelibrary.com]

from a weak stabilizing interaction between the anisyl-oxygen and the nickel(II) center. The O···Ni-distance in this complex amounts to only 2.832 (1) Å is therefore smaller than their combined van-der Waals radii (≈3.28 Å[35]). A similar effect has been observed in the structurally related complex [(dppe)Ni(*ortho*-anisyl)Br],[34] wherein the anisyl-ring stands at an angle of 88.3 (1)° relative to the coordination plane, and the O···Ni-distance (2.871 (2) Å) is also smaller than the van-der-Waals radii.

Both complexes show two sets of signals in both the ^{1}H and the ^{31}P NMR spectra, even though homo chiral phosphines (**C1**) and aryl-groups (**C2**) were introduced, respectively. Apparently, rotation of the aryl-group on the nickel center around the Ni—C bond is hindered and slow on the NMR-timescale. The hindered rotation leads to planar chirality relative to the coordination plane around the metal center. In consequence, epimeric pairs of diastereomeres are observed, that have defined stereogenic centers on the DIPAMP-ligand (**C1**) and the aryl-substituent (**C2**), respectively, but differ in the relative (*M* or *P*) configuration of the *ortho*-substituted aryl-ligand (Scheme 3). A similar behavior has been observed for related Ni(II)-aryl-complexes.[36] For **C1** the epimer-ratio is about 2:1 ratio, while for **C2** an approximate 1:1.1 ratio is observed (see Figure S8 and Figure S11 in the ESI).

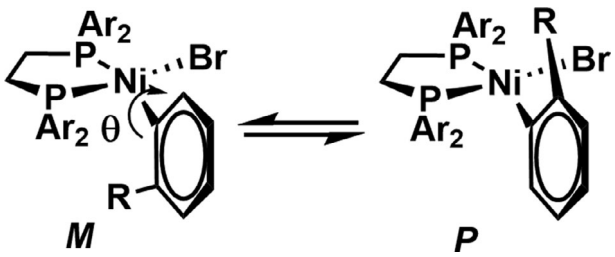

SCHEME 3 ***P*** - and ***M***-configured rotational epimers of **C1** and **C2**

Experimental determination of the rotational barrier of **C1** by variable temperature NMR is formally not possible because the rotational isomers are not chemically equal. However, it can be seen from VT-NMR data (Figure S3 in the ESI) that signals of the different methoxy-groups do not coalesce up to 358 K. At this temperature, the rotation is therefore still slow on the NMR time-scale.

In order to estimate the rotational barrier in the complexes, **C1-*RR*** has been simulated by DFT calculations at the B3LYP-D3/tzvp level (plus pseudopotentials mdf10 (Ni) and mwb28 (Br)). The rotation of the anisyl-group has been simulated via relaxed potential energy scans around the Ni—C-bond (torsion angle Θ, Br–Ni–C–C^{OMe}, Scheme 3), both in the forward (+) direction, and the backward (−) direction. Analogous to the findings from the crystal structures, the most stable conformation requires the anisyl ring to stand perpendicular to the coordination plane around the metal center, at an angle of 93.0°. The ***RRP***-configuration (Figure 2) was found to be slightly more stable than the ***RRM***-configuration. The difference (ΔG = 4.8 kJ/mol) lies within the margin of error of the calculation and therefore indicates that the epimers are very similar in energy. This is in agreement with the experimentally observed distribution of 2:1, which would require a ΔG of ca. 1.7 kJ/mol.

The rotational scan indicated rotational barriers in the range of 80–100 kJ/mol. In the most hindered

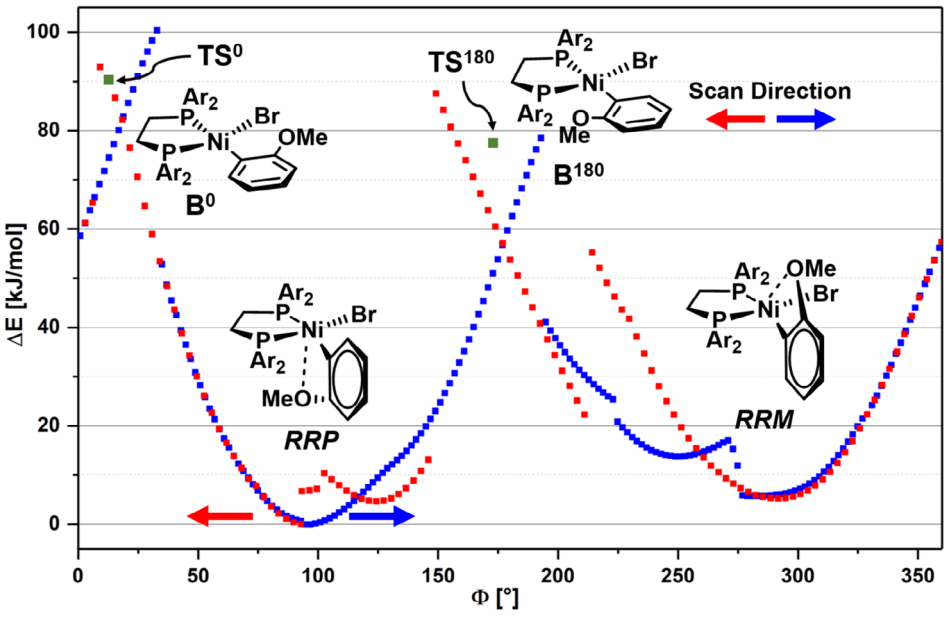

FIGURE 2 Computed energy profiles of rotational scans of **C1-*RR***. Starting point: optimized geometry of ***RRP***. : $\mathbf{TS^0}$/TS^{180}, Method: B3LYP-D3/TZVP [Color figure can be viewed at wileyonlinelibrary.com]

geometries, the anisyl-ring is required to be near coplanar to the coordination plane around nickel (i.e., $\Theta \approx 0°$ or 180°). The higher barrier (93–100.0 kJ/mol, depending on the sense of rotation) was identified for low rotational angles of 9.3° (−) and 33.0° (+) (Scheme 3, $\mathbf{B^0}$). At torsion angles of 149.2° (−) to 193.0 (+) the complex shows a lower rotational barrier of 78 to 87 kJ/mol (Scheme 3, $\mathbf{B^{180}}$).

The discontinuities in the rotational scans at $\mathbf{B^0}$ and $\mathbf{B^{180}}$ prompted us to try to locate the corresponding transitional states ($\mathbf{TS^0}$ and $\mathbf{TS^{180}}$). In agreement with the highest strains observed in the rotational scan, $\mathbf{TS^0}$ (Θ = 13.7°) is located 90.7 kJ/mol "/>"/> above the ***RRP***-epimer (and 85.9 kJ/mol above ***RRM***) and $\mathbf{TS^{180}}$ (Θ = −173.0°) lies 78.1 above the ***RRP***-epimer (73.3 kJ/mol above ***RRM***). $\mathbf{TS^0}$ exhibits a torsion angle (Br–Ni–C–C[OMe]) of 13.7°. The strain leads to a weakening of all bonds to the metal center. The bromo-ligand, is particularly affected with the Ni–Br distance changing from 2.397 Å in ***RRP*** to between 2.435 Å in $\mathbf{TS^0}$ and 2.456 Å in $\mathbf{TS^{180}}$. In both structures, the complexes avoid steric strain by adopting a tetrahedrally distorted coordination geometry at the metal center. This manifest itself, for example, in Br–Ni–P_{trans}-angles of 34.9° and 22.1° for $\mathbf{TS^0}$ and $\mathbf{TS^{180}}$ as opposed to 10.2° and 3.6° in ***RRP*** and ***RRM***, respectively.

Overall, these barriers are in the range for example, of unsubstituted 1,1′-binapthyl, which is not configurationally stable, and racemizes within hours.[37] The rotational barriers in **C1** and **C2** are therefore considered sufficiently low for slow rotation to occur at ambient temperatures.

The complexes were characterized by UV–vis and circular dichroism (CD) spectroscopy (Figure 3). The two types of complexes show very similar absorption spectra, with a weak, broad longest wavelength absorption bands (λ_{max}) centered on 422 nm (23,700 cm^{-1}). We attribute this absorption to a metal centered d-d-transition in the square planar complexes. While the transition is higher in energy than typically observed for complexes of the type [(dppe)NiX_2] (X = halogen),[38] it agrees with the absorption features of related [(L_2)Ni(*ortho*-anisyl)Br]-complexes (see Figure S1 in the ESI). Additional absorption bands, for example, at 336 nm (**C1**) and 330 nm (**C2**), and higher energies are attributed to charge-transfer processes involving the phosphine ligands. The λ_{max}-band corresponds to an onset of the absorption in solution at ca. 485 nm, and therefore at shorter wavelength than **P1** (494 nm), **P2** (520 nm), and **P3** (498 nm).[10] CD-spectra of both types of complexes showed mirror-image behavior for the respective sets of epimers. CD-effects are observed around the λ_{max}-band, while the effect is generally much more pronounced at the higher energy absorption bands. Compared to **C2**, the

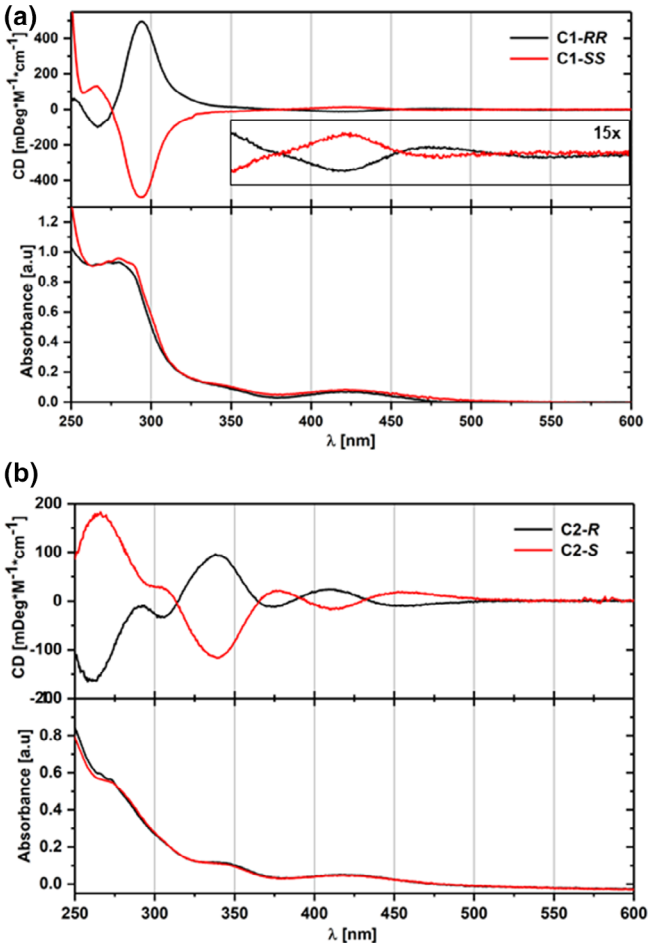

FIGURE 3 UV–vis and CD spectra of **C1** (a) and **C2** (b). All spectra recorded in THF. Insert in (a) shows an enlarged section of the CD spectrum [Color figure can be viewed at wileyonlinelibrary.com]

Cotton-effect of **C1** below 325 nm is much stronger, relative to the one of the λ_{max}-band. This is a further indication, that the transitions in this region involve the intrinsically chiral DIPAMP-ligand.[39]

3.2 | Polymer synthesis and properties

Initiation of the polymerization process in complexes of the type [L_2Ni(Ar)Hal] (**I** in Scheme 4) is well understood.[4] At first, the displacement the halide ligand from the metal center of the precatalyst occurs (**I** ⟶ **II** ⟶ **III** in Scheme 4), via an associative substitution mechanism that involves pentacoordinate Ni-species (**II**/**III**). In the cationic complex **III**, an intramolecular nucleophilic attack of the aryl-substituent on the neighboring isocyanide then yields the iminoacyl-complex **IV** via a 1,1-insertion, and a pentacoordinate complex (**V**) forms again through association of isocyanide. This formally

concludes the initiation process. Chain-extension then occurs by nucleophilic attack of the iminoacyl-carbon onto a neighboring isocyano-ligand (**V** ⟶ **VI**), and subsequent repetition of isocyanide association (**VI** ⟶ **VII**), and nucleophilic 1,1-insertion (**VII** ⟶ **VI**). The mechanism formally requires only three of the five available coordination sites and may proceed in the presence of DIPAMP and DPPE on the metal center. However, experiments showed that addition of isocyanides to solutions of [(dppe)Ni(*ortho*-anisyl)Br][34] gave only ^{31}P NMR spectra of free DPPE. The phosphine ligand is therefore displaced by the isocyanides within the timeframe of the above experiments (<5 min), and complexes of type **Va** (Scheme 4) are formed. The eventual displacement of the phosphines may be expected, since isocyanides are stronger ligands than phosphines.[3] Still, the fact that the isocyanides overcome even the chelating ligands DIPAMP and DPPE is quite surprising. In the light of findings reported herein (vide infra), the displacement most likely occurs after the initiation (after state **IV**), and quite possibly only after several rounds of chain extension (**Va** ⟶ **VIa**).

Following these deliberations, the polymerization behavior of **C1** and **C2** was investigated in more detail. Monitoring of the polymerization of **M2** with **C1-*SS*** and **C2-*S*** in toluene/THF mixtures proceeds quickly (Figure 4a,c, see also Figure S5 in the ESI). At catalyst loadings of 0.5% (**C1-*SS***) and 0.25% (**C2-*S***) respectively, number-average molecular weights (M_n) of 15–20 kg/mol, corresponding to degrees of polymerization (DP_n) of more than 30–40, were obtained within 2 min. The polymerization proceeds steadily over time and reaches quantitative monomer conversion within 3–4 hr at ambient temperature. **C1-*SS*** yielded a maximum M_n of 51.3 kg/mol (DP_n = 106, PDI = 1.24) while **C2-*S*** gave M_n = 113.6 kg/mol (DP_n = 235, PDI = 1.37). Both catalysts provide material with low PDI. However, **C2-*S*** initially yields higher PDIs (1.5–1.7 after 1–2 min), which then level off over time. This might indicate more sluggish initiation of **C2**, possibly due to the more sterically hindered aryl-moiety. Nevertheless, the linear correlation between M_n and monomer conversion confirms the presence of a chain-growth-polycondensation process for both catalysts (Figure 4b,d). These results also indicate that a significant degree of polymerization can readily be achieved within shorter reaction times than can be probed by ^{31}P NMR. The fact that only free ligand was observed by ^{31}P NMR does therefore not rule out asymmetric induction of the polymerization by **C1** as detailed in Scheme 4 (**V** ↔ **VI**).

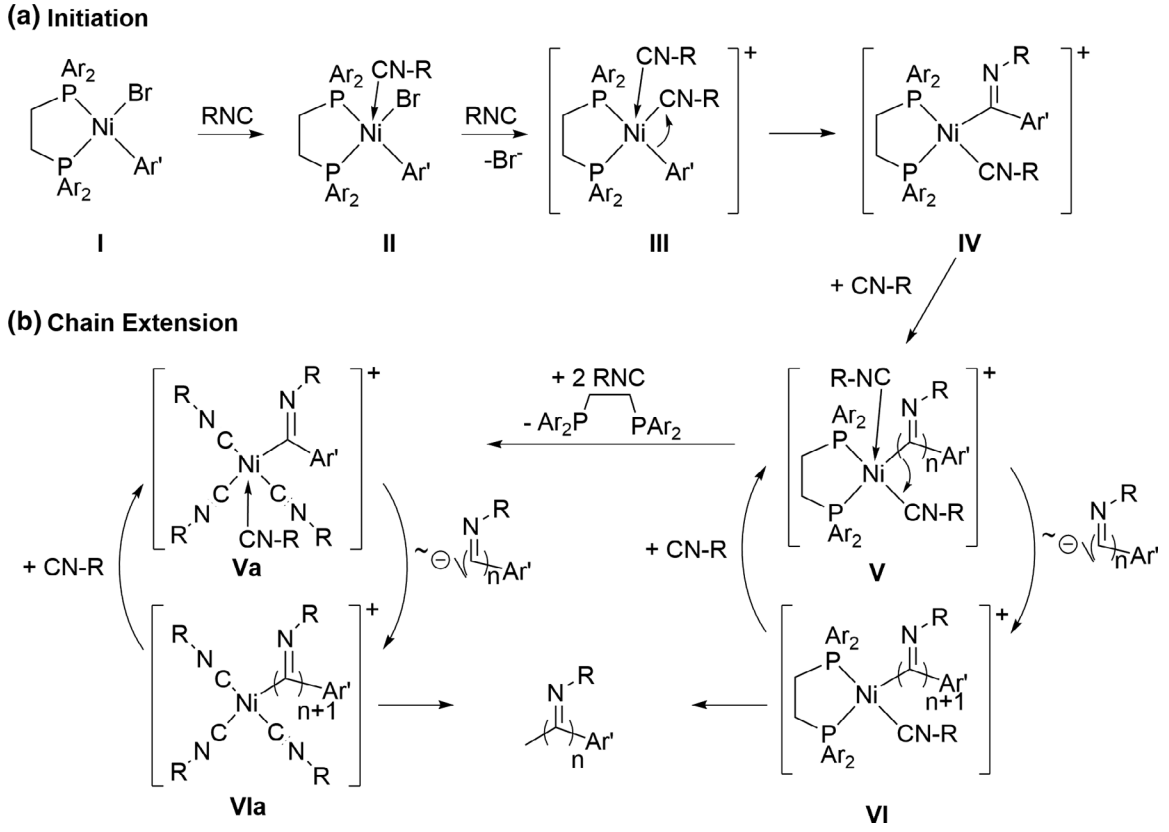

SCHEME 4 Initiation and polymerization mechanism for **C1** and **C2**. Ar/Ar′: arylgroups on phosphine ligands and nickel-pre catalyst, Ph, o-anisyl, or chiral aryl-group

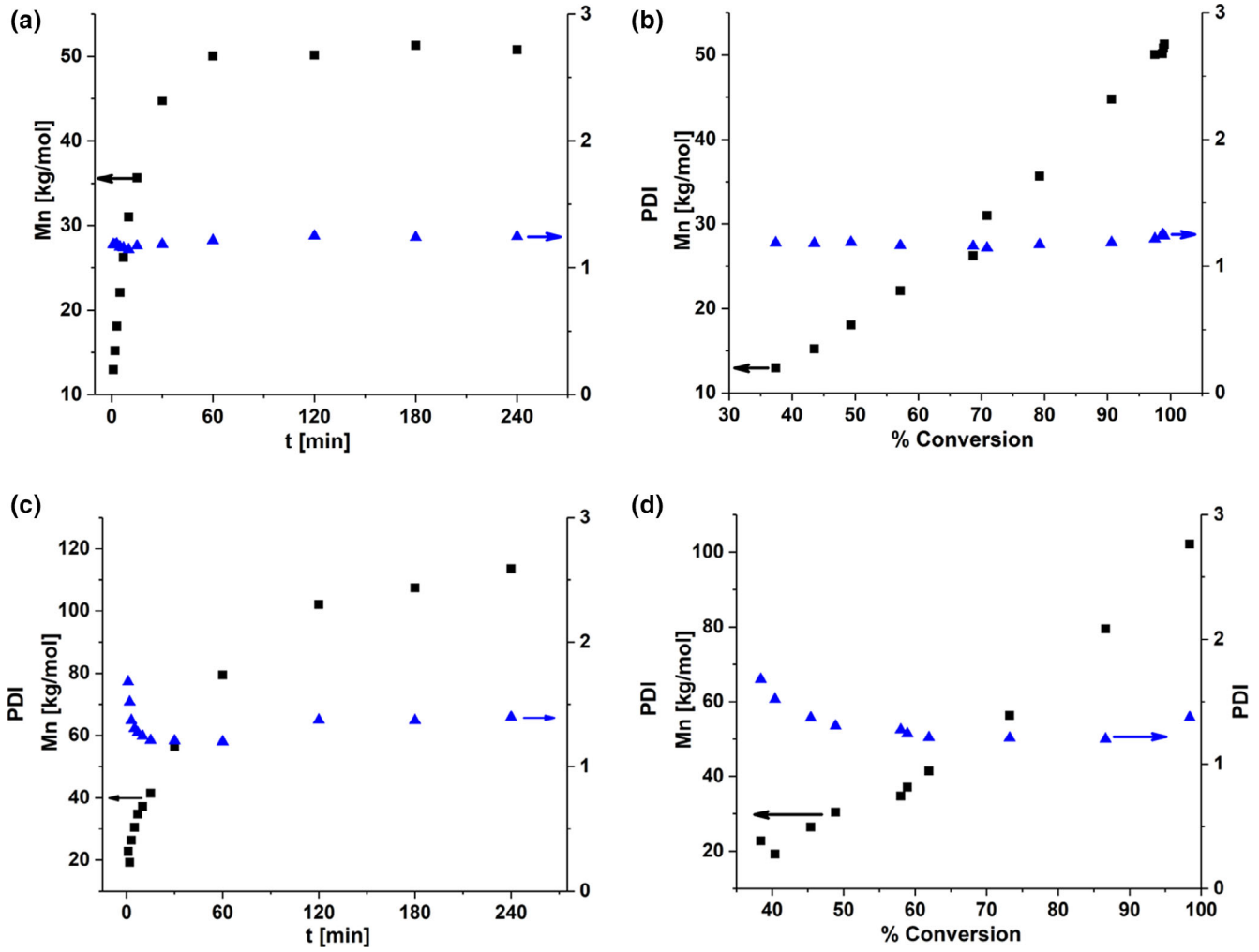

FIGURE 4 M_n and PDI versus time and versus conversion plots for the polymerization of **M2** with **C1-*SS*** (**a**, **b**, catalyst loading 0.5 mol %) and **C2-*S***. (c, d, catalyst loading 0.25 mol%) [Color figure can be viewed at wileyonlinelibrary.com]

However, analyses of polymer batches prepared with **C1** under similar conditions as the above experiment, that is, polymerization in toluene (**M2**/**M3**) or a toluene/THF solvent mixture (**M1**) gave no optically active material. An exception was **M2**/**P2**, which showed a weak non-zero optical rotation in polarimetry ($[\alpha]_D^{20} = 5.0°$ dm^{-1} L^{-1} at M_n = 19.0 kg/mol, PDI = 1.15, DP_n = 39, Catalyst: 2% **C1-*R***). One reason for this finding might have been that the polymers are not configurationally stable in good solvents and racemization occurs. This would agree with the reported solvent- and additive-dependent racemization or chiral resolution of poly(arylisocyanide)s.[4a,40] Alternatively, inversion of the sense of polymerization might randomly occur in the course of the synthesis. The latter would lead to less optically active material at higher molecular weights, which we also observed.

To prevent racemization, we therefore tested different reaction media with co-solvents (Et_2O, MeCN) wherein the neat homo polymers are insoluble. In these experiments, the batches of **P1** and **P3** showed optical activity, and the rotational angle measured for **P2** was significantly larger than observed before ($[\alpha]_D^{20} = 22.5°$ dm^{-1} L^{-1}).

Following these preliminary tests, batches of the polymers were prepared under identical conditions with enantiomeric pairs of all available catalysts (**C1-*RR***, **C1-*SS***, and **C2-*R***, **C2-*S***), and the resulting polymers were investigated by CD spectroscopy (Table 1). A catalyst loading of 1% was used to ensure the formation of high molecular weight polymers. However, aggregation and precipitation of the polymers in the employed solvent mixtures limits the maximum reachable molecular weights. For polymerizations with **C1**, polymer batches with number-average molecular weights of M_n = 3–7 kg/mol and low polydispersities (PDI ≈ 1.1) were isolated. These values correspond to degrees of polymerization of 14–17 for **P1** (Table 1, entries 1–4), 8–14 for **P2** (entries 5–8), and 10–11 for **P3** (entries

9–12). Polymerization of **M2** with **C2** gave somewhat higher molecular weights and consequently higher degrees of polymerization (**C2-*S***: M_n = 11.1 kg/mol, DP_n = 23; **C2-*R***: M_n = 13.2 kg/mol, DP_n = 27, Table 1, entries 13 and 14) at equally low PDIs.

The polymers were isolated by precipitation into methanol, followed by washing with methanol and hexane, to remove traces of catalyst or phosphine ligands. Subsequent analysis by CD-spectroscopy showed only a very weak Cotton-effect for batches of **P2** prepared with **C2** (see Figure S6 in the ESI). The asymmetric induction of the chiral end-group therefore seems to be weak. However, polymers **P1**, **P2**, and **P3** prepared with **C1** consistently showed a stronger Cotton-effect and enantiomeric catalysts gave mirror-symmetric CD-spectra (Figures 3 and 5A–C).

Polymerization with **C1-*SS*** yielded material that exhibits an initial positive Cotton-effect setting in at 475 nm (**P1**), 550 nm (**P2**), and 500 nm (**P3**), respectively. Polymer **P2** shows the lowest optical gap, with a longest-wavelength absorption band between 350 and 550 nm that originates from the absorption of the tetraphenylpentafulvene-moiety.[9,10] Since **P2** shows optical activity across the whole of the above range, we can attribute the chiroptical effect to the helical conformation of the polymer. The same is of course true for **P1** and **P3**. However, their absorption covers the same range as **C1** and **C2**. And even though absorption of the complexes in the visible range is very weak, a tainting of the samples by residual catalyst could not directly be ruled out in these cases.

To elucidate the true helical sense of the prepared polymers, the structure of an oligomeric models of **P2** (**$P2_{8M}$**, 8mer, *M*-helix) has been optimized at the B3LYP-D3/6-31G(d,p) level, and its chirooptical properties were calculated using CAM-B3LYP/6-31G(d,p).

The main chain in **$P2_{8M}$** forms a 4_1-helix and the outward peripheral fulvenyl-groups adopt at stacked orientation with their fifth neighbors. The respective cyclopentadienyl-rings are close to coplanar with angles between ring planes of 4.6° and 10.5°. The steric bulk of phenyl-rings does not allow tight stacking, however, and the Cp-rings are therefore

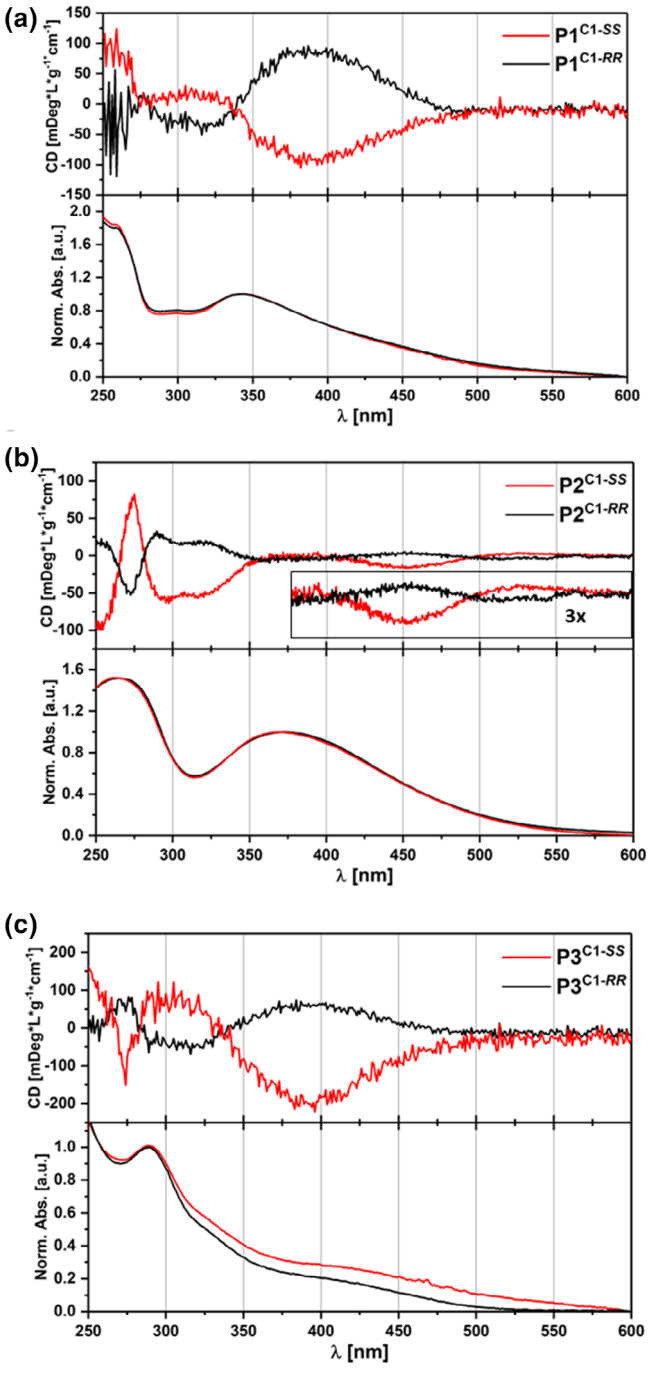

FIGURE 5 CD- and corresponding UV-spectra of polymers **P1**, **P2**, and **P3** synthesized with catalysts **C1-*SS*** and **C1-*RR***. All spectra recorded in DCM [Color figure can be viewed at wileyonlinelibrary.com]

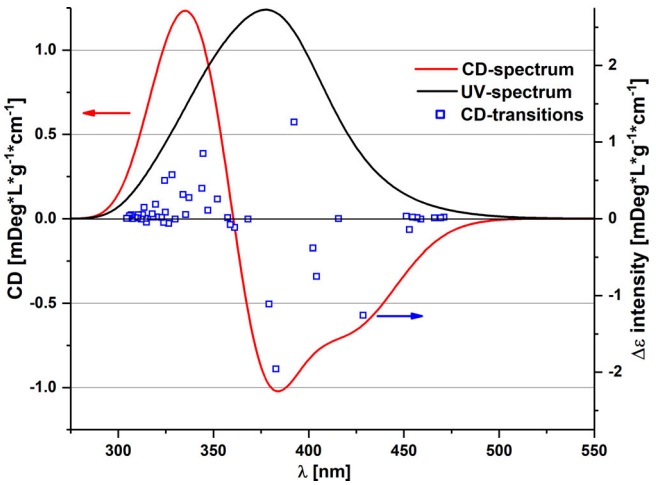

FIGURE 6 UV and CD-spectra of **$P2_{8M}$** simulated by TD-DFT. Line-width at half maximum = 0.4 eV [Color figure can be viewed at wileyonlinelibrary.com]

spaced ca. 4.6 Å apart (Cp-ring-plane to closest Cp-ring-atom) (Figure 6).

TDDFT-calculation of the first 50 excited states yielded a number of transitions with very weak but mostly positive effects between 475 and 450 nm, followed by transitions with strong negative CD-effects. The overlay of the transitions yields a CD-spectrum with an onset at 475 nm and initial negative cotton effect that leads to a maximum at 383 nm. These results are in reasonable agreement with experimental data for $\mathbf{P2}^{\mathbf{C1\text{-}SS}}$, which shows a marginal positive CD-Effect at high wavelengths, followed by a negative maximum at 451 nm. The latter value agrees with the experimental data (Figure 5b), and would indicate that $\mathbf{P2}^{\mathbf{C1\text{-}SS}}$ forms an *M*-helix.

4 | CONCLUSIONS

We have introduced new nickel precatalysts of the type [(L_2)Ni(Ar)Br], bearing either chiral chelating phosphine ligands (RR-/SS-dipamp) (**C1**) or a chiral aryl-substituent (**C2**). Polymerization experiments with the fulvenyl-functionalized **M2** showed that both catalysts reliably initiate chain-growth polymerization, and give access to high molecular weight materials (M_n 50–100 kg/mol, DP_n = 100–230). Furthermore, both catalysts allow screw-sense selective polymerization of monomer **M1**, **M2**, and **M3** to give optically active polyisocyanides **P1**–**P3**, when "bad" solvents are used which prevent racemization of the polymers in solution. The effect is moderate for **C2**, but very pronounced for **C1**. This is insofar surprising, since ^{31}P NMR experiments show that the chelating phosphine ligands are displaced by the isocyanides in the course of the polymerization. The finding that chiral spectator ligands like DIPAMP can still effect asymmetric induction opens up new strategies for the preparation of helical **PIC**s. Furthermore, we have demonstrated that precatalysts of the type **C1** and **C2** can be readily prepared by the reported procedure. This offers a much more convenient access to precatalysts bearing chiral initiating groups, compared to previously reported methods,[41] and will therefore allow to expand this field of research much more rapidly.

ACKNOWLEDGMENTS

SS, JT, and FP thank the German Science Foundation (DFG, German Research Foundation, project number FP 2217/3-1) and the Fonds der Chemischen Industrie (FCI, Liebig scholarship to FP) for financial support. This work has also been funded by the Deutsche Forschungsgemeinschaft (DFG) under Germany's Excellence Strategy (EXC-2033/project number 390677874). CM furthermore acknowledges support by the DFG through the Heisenberg program (ME 4267/5-1/project number 418661145). NMK has been supported by a doctoral fellowship of the FCI.

ORCID

Andreas Orthaber https://orcid.org/0000-0001-5403-9902

Christian Merten https://orcid.org/0000-0002-4106-1905

Frank Pammer https://orcid.org/0000-0002-3869-0196

REFERENCES

[1] a) I. Ugi, S. Lohberger, R. Karl, *Comp. Org. Synth.* **1991**, *2*, 1083. b) I. Ugi, B. Werner, A. Dömling, *Molecules* **2003**, *8*, 53.

[2] a) S. Lang, *Chem. Soc. Rev.* **2013**, *42*, 4867. b) G. Qiu, Q. Ding, J. Wu, *Chem. Soc. Rev.* **2013**, *42*, 5257.

[3] a) P. D. Harvey, *Coord. Chem. Rev.* **2001**, *219–221*, 17. b) E. Singleton, H. E. Oosthuizen, *Adv. Organomet. Chem.* **1983**, *22*, 209. c) Y. Yamamoto, *Coord. Chem. Rev.* **1980**, *32*, 193. d) P. M. Treichel, *Adv. Organomet. Chem.* **1973**, *11*, 21.

[4] a) E. Schwartz, M. Koepf, H. J. Kitto, R. J. M. Nolte, A. E. Rowan, *Polym. Chem.* **2011**, *2*, 33. b) Y. Nagata, M. Suginome, in *Polyisocyanides, Poly(quinoxaline-2,3-diyl)s, and Related Helical Polymers Used as Chiral Polymer Catalysts in Asymmetric Synthesis in Polymeric Chiral Catalyst Design and Chiral Polymer Synthesis.* (Ed: S. Itsuno), John Wiley and Sons, Hoboken **2011**, p. 223. c) R. J. M. Nolte, *Chem. Soc. Rev.* **1994**, *23*, 11. d) W. Drenth, R. Nolte, *Acc. Chem. Res.* **1979**, *15*, 30. e) F. Millich, *Chem. Rev.* **1972**, *72*, 101.

[5] a) X. Yan, S. Zhang, D. Peng, P. Zhang, J. Zhi, X. Wu, L. Wang, Y. Dong, X. Li, *Polym. Chem.* **2018**, *9*, 984. b) Y.-X. Xue, J.-L. Chen, Z.-Q. Jiang, Z. Yu, N. Liu, J. Yin, Y.-Y. Zhu, Z.-Q. Wu, *Polym. Chem.* **2014**, *5*, 6435. c) K. Onitsuka, T. Mori, M. Yamamoto, F. Takei, S. Takahashi, *Macromolecules* **2006**, *39*, 7224. d) K. Onitsuka, K. Yanai, F. Takei, T. Joh, S. Takahashi, *Organometallics* **1994**, *13*, 3862.

[6] a) Z.-Q. Wu, J. D. Radcliffe, R. J. Ono, Z. Chen, Z. Li, C. W. Bielawski, *Polym. Chem.* **2012**, *3*, 874. b) Z.-Q. Q. Wu, D.-F. F. Liu, Y. Wang, N. Liu, J. Yin, Y.-Y. Y. Zhu, L.-Z. Z. Qiu, Y.-S. S. Ding, *Polym. Chem.* **2013**, *4*, 4588. c) Z. Yu, N. Liu, L. Yang, Z. Jiang, Z. Wu, *Macromolecules* **2017**, *50*, 3204. d) Z.-Q. Wu, R. J. Ono, Z. Chen, C. W. Bielwaski, *J. Am. Chem. Soc.* **2010**, *132*, 14000. e) M. Su, N. Liu, Q. Wang, H. Wang, J. Yin, Z.-Q. Wu, *Macromolecules* **2016**, *49*, 110. f) N. Liu, C.-G. Qi, Y. Wang, D. F. Liu, J. Yin, Y.-Y. Zhu, Z.-Q. Wu, *Macromolecules* **2013**, *46*, 7753.

[7] N. Hida, F. Takei, K. Onitsuka, K. Shiga, S. Asaoka, T. Iyoda, S. Takahashi, *Angew. Chem. Int. Ed.* **2003**, *42*, 4349.

[8] a) E. Gomar-Nadal, L. Mugica, J. Vidal-Gancedo, J. Casado, J. T. L. Navarrete, J. Veciana, C. Rovira, D. B. Amabilino, *Macromolecules* **2007**, *40*, 7521. b) E. Gomar-Nadal, J. Veciana, C. Rovira, D. B. Amabilino, *Adv. Mater.* **2005**, *17*, 2095.

[9] S. Schraff, Y. Sun, A. Orthaber, F. Pammer, *Eur. J. Inorg. Chem.* **2019**, *2019*, 42.

[10] S. Schraff, Y. Sun, F. Pammer, *Macromolecules* **2018**, *51*, 5323.

[11] E. Yashima, K. Maeda, H. Iida, Y. Furusho, K. Nagai, *Chem. Rev.* **2009**, *109*, 6102.

[12] R. J. M. Nolte, A. J. M. Van Beijnen, W. Drenth, *J. Am. Chem. Soc.* **1974**, *96*, 5932.

[13] K. Maeda, M. Ishikawa, E. Yashima, *J. Am. Chem. Soc.* **2004**, *126*, 15161.
[14] F. Millich, G. K. Baker, *Macromolecules* **1969**, *2*, 122.
[15] T. Harada, M. C. Cleij, R. J. M. Nolte, A. M. F. Hezemans, W. Drenth, *J. Chem. Soc. Chem. Commun.* **1984**, 726.
[16] T. Kajitani, K. Okoshi, S. Sakurai, J. Kumaki, E. Yashima, *J. Am. Chem. Soc.* **2006**, *128*, 708.
[17] L. Xu, L. Yang, Z. Guo, N. Liu, Y.-Y. Zhu, Z. Li, Z.-Q. Wu, *Macromolecules* **2019**, *52*, 5698.
[18] T. J. Deming, B. M. Novak, *J. Am. Chem. Soc.* **1992**, *114*, 7926.
[19] T. J. Deming, B. M. Novak, *J. Am. Chem. Soc.* **1992**, *114*, 4400.
[20] P. C. J. Kamer, M. C. Cleij, R. J. M. Nolte, T. Harada, A. M. F. Hezemans, W. Drenth, *J. Am. Chem. Soc.* **1988**, *110*, 1581.
[21] P. C. J. Kamer, R. J. M. Nolte, W. Drenth, *J. Chem. Soc. Chem. Commun.* **1988**, *1789–1791*.
[22] P. C. J. Kamer, R. J. M. Nolte, W. Drenth, *J. Am. Chem. Soc.* **1988**, *110*, 6818.
[23] L. Xu, X.-H. Xu, N. Liu, H. Zou, Z.-Q. Wu, *Macromolecules* **2018**, *51*, 7546.
[24] O. Coulembier, M. Surin, A. Mehdi, R. Lazzaroni, R. C. Evans, P. Dubois, *Chem. Commun.* **2016**, *52*, 171.
[25] R. J. Ono, A. D. Todd, Z. Hu, D. A. Vanden Bout, C. W. Bielawski, *Macromol. Rapid Commun.* **2014**, *35*, 204.
[26] S. Schraff, S. Maity, L. Schleeper, Y. Dong, S. Lucas, A. A. Bakulin, E. von Hauff, F. Pammer, *Polym. Chem.* **2020**, *11*, 1852. https://doi.org/10.1039/C9PY01879D.
[27] J. Lee, S. Shin, T.-L. Choi, *Macromolecules* **2018**, *51*, 7800.
[28] T. Yamada, M. Suginome, *Macromolecules* **2010**, *43*, 3999.
[29] W. L. F. Armarego, D. D. Perrin, *Purification of Laboratory Chemicals*, 4th ed., Butterworth-Heinemann, Oxford **1997**.
[30] G. R. Fulmer, A. J. M. Miller, N. H. Sherden, H. E. Gottlieb, A. Nudelman, B. M. Stoltz, J. E. Bercaw, K. I. Goldberg, *Organometallics* **2010**, *29*, 2176.
[31] A. Altomare, G. Cascarano, C. Giacovazzo, A. Guagliardi, M. C. Burla, G. Polidori, M. Camalli, *J. Appl. Cryst.* **1994**, *27*, 435.
[32] G. M. Sheldrick, *Acta Cryst.* **2008**, *A64*, 112.
[33] M. J. Frisch, G. W. Trucks, H. B. Schlegel, G. E. Scuseria, M. A. Robb, J. R. Cheeseman, G. Scalmani, V. Barone, G. A. Petersson, H. Nakatsuji, X. Li, M. Caricato, A. V. Marenich, J. Bloino, B. G. Janesko, R. Gomperts, B. Mennucci, H. P. Hratchian, J. V. Ortiz, A. F. Izmaylov, J. L. Sonnenberg, D. Williams-Young, F. Ding, F. Lipparini, F. Egidi, J. Goings, B. Peng, A. Petrone, T. Henderson, D. Ranasinghe, V. G. Zakrzewski, J. Gao, N. Rega, G. Zheng, W. Liang, M. Hada, M. Ehara, K. Toyota, R. Fukuda, J. Hasegawa, M. Ishida, T. Nakajima, Y. Honda, O. Kitao, H. Nakai, T. Vreven, K. Throssell, J. A. Montgomery Jr., J. E. Peralta, F. Ogliaro, M. J. Bearpark, J. J. Heyd, E. N. Brothers, K. N. Kudin, V. N. Staroverov, T. A. Keith, R. Kobayashi, J. Normand, K. Raghavachari, A. P. Rendell, J. C. Burant, S. S. Iyengar, J. Tomasi, M. Cossi, J. M. Millam, M. Klene, C. Adamo, R. Cammi, J. W. Ochterski, R. L. Martin, K. Morokuma, O. Farkas, J. B. Foresman, D. J. Fox, *Gaussian 16, Revision C.01*, Gaussian, Inc, Wallingford, CT **2016**.
[34] F. Pammer, J. Jäger, B. Rudolf, Y. Sun, *Macromolecules* **2014**, *47*, 5904.
[35] S. S. Batsanov, *Inorg. Mater.* **2001**, *37*, 871.
[36] E. A. Standley, S. J. Smith, P. Müller, T. F. Jamison, *Organometallics* **2014**, *33*, 2012.
[37] L. Meca, D. Reha, Z. Havlas, *J. Org. Chem.* **2003**, *68*, 5677.
[38] a) I. M. Angulo, E. Bouwman, M. Lutz, W. P. Mul, A. L. Spek, *Inorg. Chem.* **2001**, *40*, 2073. b) G. R. Van Hecke, D. J. Horrocks, *Inorg. Chem.* **1968**, *5*, 1968.
[39] Minor deviations between the UV-vis and CD-spectra of **C1-*SS*** and **C1-*RR*** are owed to inadvertent decomposition during measurements under air. See Figure S2 in the ESI for monitoring of the gradual decomposition of **C1-*SS***.
[40] M. Ishikawa, K. Maeda, Y. Mitsutsuji, E. Yashima, *J. Am. Chem. Soc.* **2004**, *126*, 732.
[41] Y. Ito, E. Ihara, M. Murakami, *Polym. J.* **1992**, *24*, 1349.

SUPPORTING INFORMATION

Additional supporting information may be found online in the Supporting Information section at the end of this article.

How to cite this article: S Schraff, NM Kreienborg, J Trampert, et al. Asymmetric chain-growth synthesis of polyisocyanide with chiral nickel precatalysts. *J Polym Sci.* 2020;58:2221–2233. https://doi.org/10.1002/pol.20200153